

TECHNICAL NOTE

Terminal densities

G. A. NARSILIO* and J. C. SANTAMARINA†

KEYWORDS: compaction; deformation; dynamics; fabric/structure of soils; liquefaction; repeated loading; settlement

INTRODUCTION

Temperature and pressure determine the state of matter. The three standard states exhibit very different geometric and density characteristics: solids have their own shape and density; liquids keep their density, but acquire the geometry of the container; and gases have neither a fixed geometry nor density, so they can fill a container of any size and shape.

Soils, and all particulates in general, behave like no other material at any phase condition. A soil mass responds as a solid when confined, flows like a liquid on a ramp, and may be stable in a wide range of possible densities (Savage, 1994; Buchanan, 2003; Corwin *et al.*, 2005; van Hecke, 2005). Therefore it is not possible to define a characteristic density for a soil (Buchanan, 2003; Umbanhowar, 2003).

Volume change in soils is the result of various particle-level mechanisms. Contact deformation prevails in small-strain deformation. This is a constant-fabric process, and the terminal density will reflect the initial fabric.

Starting at intermediate strains, chain buckling and slip-down cause increased interparticle coordination; eventually rotational frustration arises, and the granular medium either deforms by contact slippage or expands against the confinement p' to facilitate particle rolling (Dafalias, 1993; Ishihara, 1996; Mueth *et al.*, 2000; Santamarina *et al.*, 2001). The balance between these coexisting and competing mechanisms determines the confinement-dependent terminal density for intermediate-to-large-strain processes. The critical-state void ratio $e_{cs} = f(p')$ is a well-recognised example of terminal void ratio e_T , in this case associated to large-strain monotonic shear (Fig. 1; Casagrande, 1936; Taylor, 1948; Schofield & Wroth, 1968; Oda & Kazama, 1998; the implications of localisation are discussed in Desrues *et al.*, 1996).

$$e_{cs} = e_{cs}^{1 \text{ kPa}} - \lambda \log\left(\frac{p'}{1 \text{ kPa}}\right) \quad (1)$$

Note that different stress histories, such as axial compression or lateral extension, cause different granular flow regimes, resulting in distinct terminal densities in monotonic loading (for numerical evidence see Chantawarangul, 1993; for a

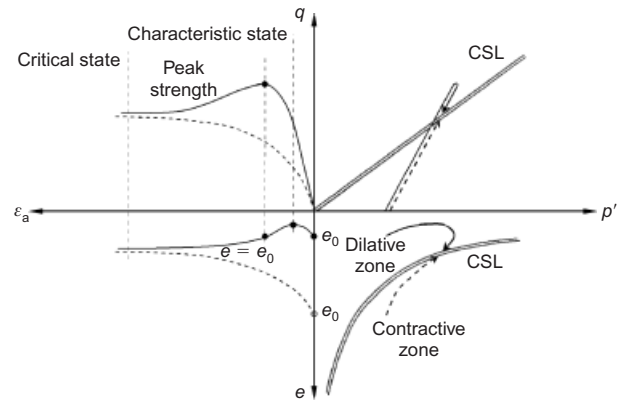


Fig. 1. Critical state: terminal void ratios under monotonic shear. Typical stress–strain–volume response for contractive (dashed lines) and dilatative (continuous lines) specimens

review of strength anisotropy in compression and extension see Santamarina, 2002).

Furthermore, soils reach a characteristic constant density when subjected to constant boundary loads (contact creep and grain crushing included), repetitive vibrations (Nowak *et al.*, 1998), or cyclic loading (Lackenby *et al.*, 2007). Even the procedurally defined minimum and maximum void ratios represent the terminal densities that are associated to the processes prescribed by the standards, that is, load and vibration in ASTM D 4253, funnelling or scooping in ASTM D 4254.

These examples suggest that every soil eventually reaches a unique terminal density and associated internal fabric that allows for the continuation of the process at constant volume. In general, the terminal density depends on the applied confinement; in addition, the terminal density will reflect the initial soil fabric when the imposed strain level does not exceed some threshold strain required for soil restructuring. The following section explores the concept of terminal density (or terminal void ratio) in cyclic processes.

TERMINAL VOID RATIO IN CYCLIC DRAINED LOADING

Different terminal densities are expected in repetitive cyclic loading as a function of the imposed cyclic strain amplitude, in agreement with the previous discussion on particle-level deformation mechanisms. This hypothesis is explored next using numerical and experimental approaches.

Numerical simulation

Consider dense sand subjected to cyclic loading to constant peak cyclic strain. Each strain cycle promotes densification under drained conditions if the strain level is larger than the volumetric threshold strain (Vucetic *et al.*, 1991) but smaller or similar to the strain at the characteristic state (Fig. 1; Luong, 1980).

Manuscript received 31 May 2007; revised manuscript accepted 17 April 2008.

Discussion on this paper closes on 1 April 2009, for further details see p. ii.

* Department of Civil and Environmental Engineering, The University of Melbourne, Parkville, Australia.

† School of Civil and Environmental Engineering, Georgia Institute of Technology, Atlanta, USA.

The NorSand model is selected to simulate this process (Jefferies & Shuttle, 2002, 2005). The simulation sequence follows.

- (a) The specimen with initial void ratio $e_0^{<0>}$ is subjected to drained axial compression loading to a selected strain level.
- (b) Axial unloading follows.
- (c) Then a new axial compression cycle starts.

The process is repeated for multiple cycles. For simplicity, it is assumed that unloading takes place at constant volume (Fig. 2(a)). In this particular process, ‘one event’ is defined as one full cycle.

The simulated sand has an initial void ratio of $e_0 = 0.785$, and it is subjected to an initial mean effective stress $p'_0 = 100$ kPa (sand parameters: $e_{cs}^{1 \text{ kPa}} = 0.86$; slope $\lambda = 0.032$ in base 10; rigidity index $I_r = 600$; Poisson’s ratio $\nu = 0.2$). The first 20 events gathered for different peak cyclic strains $\epsilon_a = 0.005, 0.015$ and 0.050 are shown in Fig. 2. Fig. 3 summarises the evolution in void ratio with respect

to the number of events for the three strain amplitudes, and for two initial void ratios $e_0 = 0.785$ and $e_0 = 0.750$.

The void ratio gradually evolves towards the corresponding terminal void ratio in all cases. The terminal void ratio e_T is determined by the strain level: the smaller the cyclic strain amplitude, the lower the terminal void ratio, yet the higher the number of cycles required to attain it (this explains the crossing of trends in Fig. 3). Note that the initial void ratio is smaller than the critical-state void ratio for the six simulated conditions $e_0 < e_{cs}$, yet the terminal void ratios for the three strain levels are $e_T < e_{cs}$. One specimen has a terminal void ratio higher than the initial void ratio $e_T > e_0$ for the imposed cyclic strain, and it dilates to reach the terminal density.

Experimental study

A parallel study is attempted using Nevada sand ($D_{50} = 0.16$ mm, $C_u = 1.8$, $e_{min} = 0.511$, $e_{max} = 0.894$). Saturated specimens are confined in a triaxial cell at an

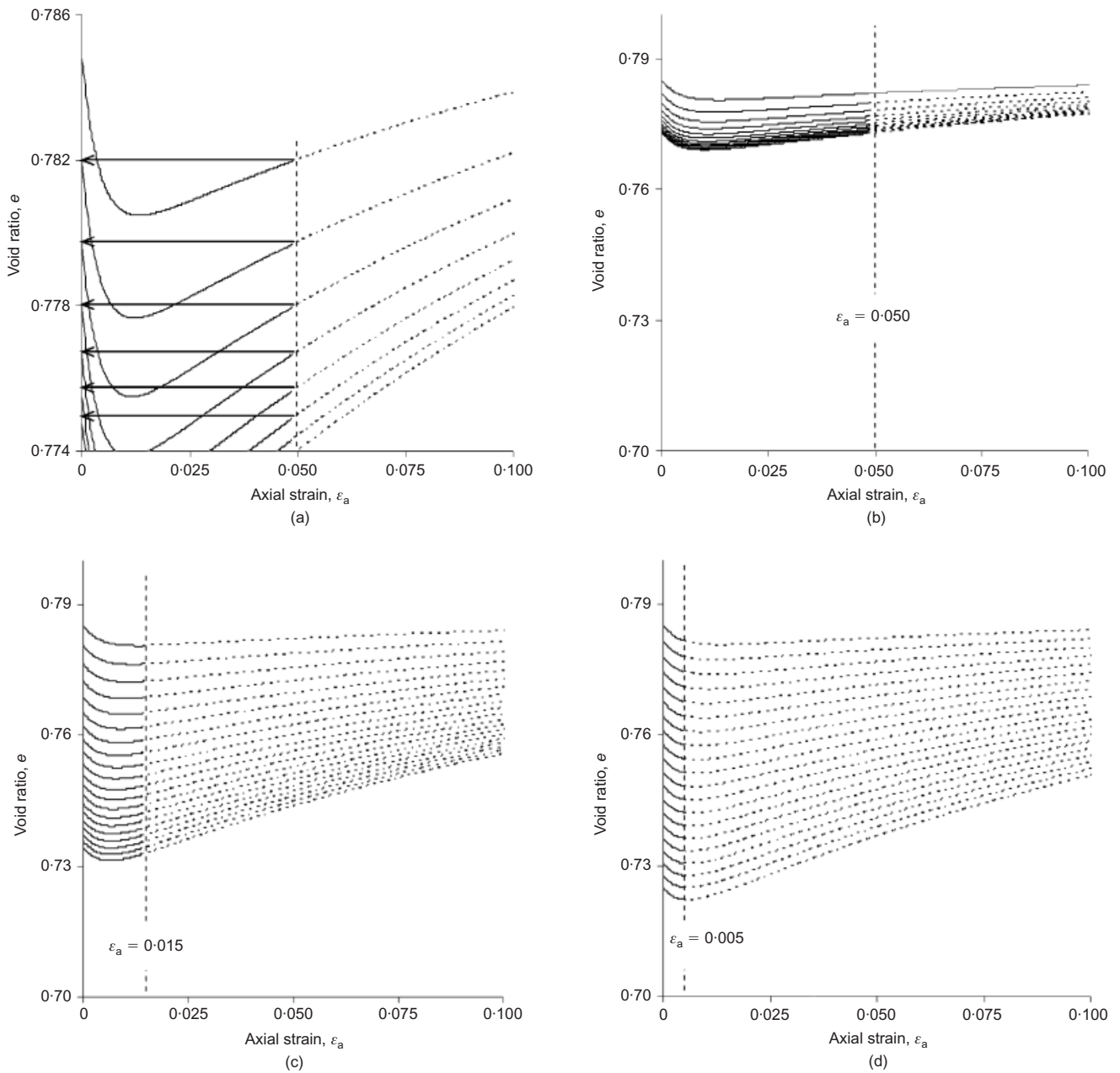


Fig. 2. Numerical cyclic strain tests (NorSand model): (a) detail of constant-volume reversal hypothesis, first 20 cycles at constant peak cyclic axial strain; (b) $\epsilon_a = 0.050$; (c) $\epsilon_a = 0.015$; (d) $\epsilon_a = 0.005$

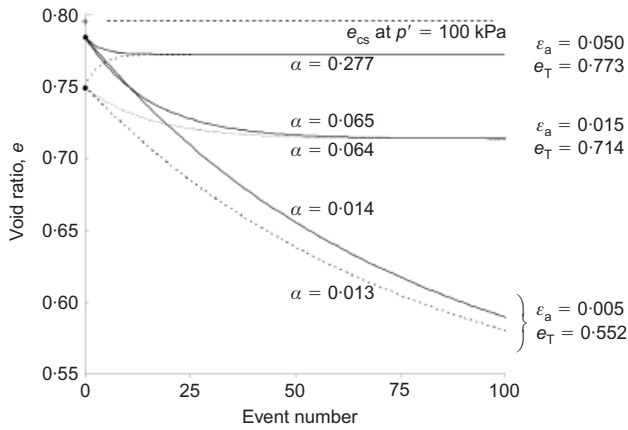


Fig. 3. Void ratio evolution against number of events for different peak cyclic strain levels: $\epsilon_a = 0.005$, $\epsilon_a = 0.015$ and $\epsilon_a = 0.050$ (NorSand model). Trends are computed for two initial void ratios: $e_0 = 0.785$ (solid lines) and $e_0 = 0.750$ (dashed lines). The critical-state void ratio that corresponds to this initial confining stress is $e_{cs} = 0.796$. The inverted values for terminal void ratios e_T and convergence rate α (equation (2)) are indicated for each case

isotropic effective stress of $p'_0 = 100$ kPa and subjected to drained cyclic loading to a predetermined axial strain amplitude (2 cycles per minute). Changes in volume are accurately measured using a pipette.

Figure 4 shows the evolution in void ratio for two levels of peak-to-peak cyclic strain, $\epsilon_a = 0.050$ and $\epsilon_a = 0.015$. Similar to the numerical results, the most pronounced volumetric changes take place during the early cycles, and gradually diminish as the void ratio asymptotically approaches the terminal void ratio corresponding to each strain level.

TERMINAL VOID RATIO IN CYCLIC UNDRAINED LOADING: POST EARTHQUAKE SETTLEMENT

Large-strain dilative soils can experience high pore water pressure generation if cyclic strains of proper amplitude are imposed (Castro, 1969; Ishihara *et al.*, 1975; Ishihara, 1985). This phenomenon is herein revisited in the context of terminal void ratios.

Strain-controlled, axial compression, cyclic triaxial tests are performed on specimens prepared with three different sands: Nevada sand, Ottawa sand and Ticino sand (properties

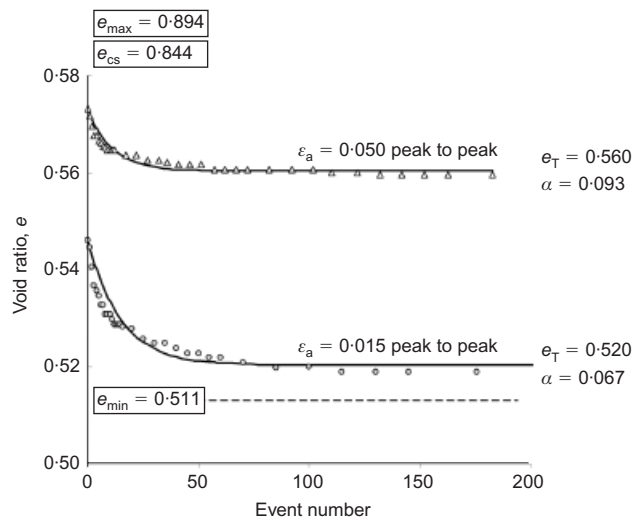


Fig. 4. Approaching terminal density in 'drained cyclic loading' events. Void ratio evolution against number of cycles for two peak-to-peak axial strain levels (triaxial cell, Nevada sand, $p'_0 = 100$ kPa, $e_{cs} = 0.844$)

are summarised in Table 1). Specimens are prepared at low void ratios so that their large-strain response is dilative at the applied isotropic effective confinement of 100 kPa. Each single 'event' consists of the following procedure.

- (a) Strain-controlled axial loading cycles are imposed under undrained conditions at constant peak-to-peak axial strain $\epsilon_a = 0.005$.
- (b) The strain cycles are repeated until either the excess pore pressure u_e equals the confining pressure σ_0 or 40 cycles are reached.
- (c) Then drainage is allowed, and the change in volume is measured using a pipette.

The same specimen is subjected to multiple similar 'events'. The change in volume after drainage is plotted as a function of event number in Fig. 5. Similar studies are conducted with Nevada sand, Ottawa sand and Ticino sand for different confining stress levels and cyclic strain amplitudes. All 11 specimens are on the dilative side of critical state, including five very dense specimens with $e_0 \approx e_{min}$; yet cyclic events at small-to-intermediate strains systematically cause positive pore pressure generation followed by volume contraction during drainage (also observed by Youd, 1984; Scott, 1986;

Table 1. Material properties for the various tested sands

Material	e_{min}	e_{max}	$\gamma_{d,max}$: kN/m ³	$\gamma_{d,min}$: kN/m ³	G_s	Critical-state parameters
Nevada sand $D_{50} = 0.16$ mm $C_u = 1.8$	0.511	0.894	17.33	13.87	2.68	$\phi_{cs} = 31^\circ$ $e_{CS}^{1\text{ kPa}} = 1.00$ $\lambda = 0.077$
Ottawa sand 20–30 $D_{50} = 0.72$ mm $C_u = 1.4$	0.50	0.80	17.33	14.44	2.65	$\phi_{cs} = 31^\circ$ $e_{CS}^{1\text{ kPa}} = 0.74$ $\lambda = 0.053$
Manufactured sand $D_{50} = 0.21$ mm $C_u = 2.8$	–	0.77	–	14.7	2.66	$\phi_{cs} = 38^\circ$
Ticino sand $D_{50} = 0.58$ mm $C_u = 1.5$	0.574	0.99	16.56	13.1	2.66	$\phi_{cs} = 37^\circ$ $e_{CS}^{1\text{ kPa}} = 1.05$ $\lambda = 0.053$

D_{50} , mean particle diameter; C_u , coefficient of uniformity; e_{min} and e_{max} , minimum and maximum void ratio; G_s , specific gravity; ϕ_{cs} , critical-state friction angle; γ_d , dry unit weight; $\gamma_{d,min/max} = \gamma_w G_s / (e_{max/min} + 1)$

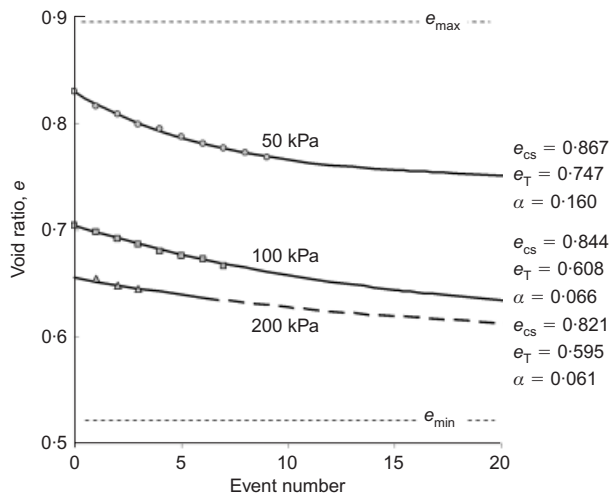


Fig. 5. Approaching terminal density in ‘liquefaction drainage’ events. Void ratio as a function of the number of events for different confining stress levels: Nevada sand. The critical-state void ratio and inverted values for terminal void ratios e_T and convergence rate α (equation (2)) are indicated in each case

Lee & Santamarina, 2007). Once again, the change in volume decreases as the number of events increases.

These results show that successive seismic events can cause repeated occurrences of large excess pore pressure generation, even in soils that are dilative under large-strain monotonic loading. The phenomenon could be disregarded if one assumes that such soils would eventually dilate should failure and large-strain shear arise; however, the existence of zones with hydraulic conductivity contrast within the medium may lead to the formation of water gaps and the complete loss of shear strength at the interlayer (Youd, 1984; Fiegel & Kutter, 1994; Kokusho & Kojima, 2002).

The volume contraction observed after each event in Fig. 5 is analogous to earthquake-induced settlements documented after seismic events: examples include a 6.4 cm settlement after the 1971 San Fernando Earthquake (peak acceleration 0.45g; Seed & Silver, 1972), and 20–50 cm settlement in Port and Rokko Islands after the 1995 Kobe earthquake (extensive liquefaction; Özkan *et al.*, 1996; Soga, 1998).

What is the potential future settlement at the same location should a similar seismic event occur? A small-scale 1g experimental study is conducted using a Plexiglas cell

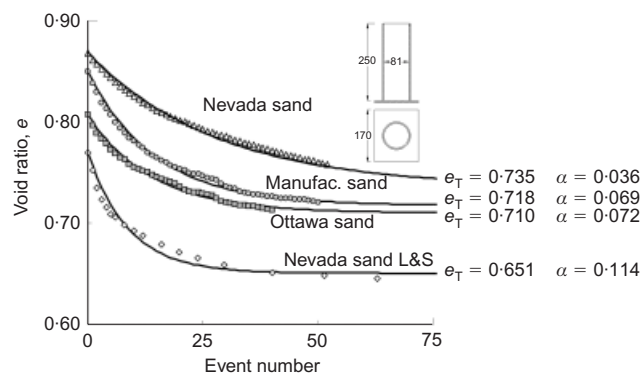


Fig. 6. Void ratio evolution in small-scale, 1g liquefaction tank studies. Each event consists of a high-energy side impact followed by re-sedimentation. Fitting parameters e_T and α for equation (2) are shown to the right; material parameters are listed in Table 1. Nevada sand L&S (open rhombi): refer to Lee & Santamarina (2007) for configuration details and internal monitoring data

(ID = 81 mm, $H = 250$ mm; Fig. 6 insert). The sand specimen is prepared by the water pluviation method (the properties of the selected sands are listed in Table 1). Then the plunger of a vertical LVDT is allowed to rest on a perforated light disc that sits on the surface of the sand bed. The dynamic event is simulated with a repeatable lateral impact at the base, generated by the pendular motion of a mass hanging from the ceiling. Repeatability is verified using an accelerometer mounted on the base near the impact point. Each impact is an ‘event’, and it is repeated every 1 min. Results in Fig. 6 show that specimens evolve towards the terminal density condition that corresponds to each soil for the given dynamic excitation, boundary conditions and stress level. In all cases a relatively large number of liquefaction events takes place. Results by Lee & Santamarina (2007) are superimposed in Fig. 6 (lower trend: open rhombi); concurrent geophysical and pore water pressure measurements gathered in that study confirmed the repetition of multiple liquefaction events before reaching the asymptotic conditions called ‘terminal void ratio’ in this paper.

ANALYSIS, DISCUSSION AND GENERALISATION

The void ratio evolution in all processes reported in this study can be fitted with an exponential function in terms of the number of events: the void ratio after the i th event e_i can be predicted from the initial void ratio e_0 by

$$e_i = e_T + (e_0 - e_T) \exp(-\alpha i) \quad (2)$$

Therefore there are two parameters for the given soil and process: the terminal void ratio e_T , and the exponent α , which captures the rate of convergence towards the terminal density. The inferred values of e_T and α for the numerical and experimental cases reported above are superimposed in Figs 3–6.

The results in Fig. 5 appear to indicate a lower terminal void ratio with increasing confining stress, in agreement with the monotonic critical state. The rate of convergence α decreases as the imposed strain level decreases (Figs 3 and 4), because the volume change per event is smaller.

The rate of convergence implies the number of events required to achieve terminal conditions. Indeed, equation (2) can be rewritten as

$$\frac{e_i - e_T}{e_0 - e_T} = \exp(-\alpha i) \quad (3)$$

Hence about 63% of the transition from the initial void ratio towards the terminal density ($e_T - e_0$) is completed when the number of events is $i_{63\%} \approx 1/\alpha$. The values of α observed in this study range from ~ 0.01 to 0.20. Therefore $i_{63\%}$ varies between 5 and 100 events for the processes studied here.

On the bases of numerical and experimental results, it is anticipated that the fastest rate of densification would be achieved by straining the soil to the smallest void ratio in each cycle, that is, just before the initiation of dilation at the characteristic state (Fig. 1). In the case of numerical results, this observation is a consequence of the zero volume change reversal assumed in simulations; however, experimental results indicate that this is a realistic general guideline. The strain level to the minimum void ratio decreases with density, that is, as the number of events increases (trends in Fig. 2; data in Tokimatsu & Seed, 1987). Therefore optimal densification requires continuous monitoring and feedback control.

We anticipate a lower bound (‘line of certain dilation’—a geometric limit) and an upper bound (‘line of certain contraction’—a stability limit) to all possible terminal void

ratios for a given granular material. In between these bounds we find e_{\max} , the normally consolidated line, the critical-state line, attainable densities in laboratory and field compaction, e_{\min} , and terminal densities for any other process. Note that grain crushing also attains terminal density; yet the new material has a different grain shape and size distribution. Similarly, grain dissolution–reprecipitation leads to its own very low terminal density, however, the new granular material has a changed particle size distribution and mineralogy. (For example, aeolically transported volcanic ash $e \approx 0.8$ –1 dissolves and reprecipitates in situ into volcanic ash soils $e \approx 2$ –71 Herrera *et al.*, 2006).

The concept of process-dependent terminal void ratio has implications in densification for any type of excitation, ranging from standard compaction (Bement & Selby, 1997), traffic (Drabkin *et al.*, 1996; Lackenby *et al.*, 2007) and pile installation (Cudmani & Gudehus, 1999) to blast densification (Narin van Court & Mitchell, 1998).

CONCLUSIONS

There is a terminal density or terminal void ratio for every soil and every process. It is presumed that there is a unique fabric associated to each terminal void ratio that supports the continuation of the process at constant volume (observed in critical state). All possible terminal void ratios for a given granular material are bounded between a state of ‘certain dilation’ (a geometric limit) and a state of ‘certain contraction’ (a stability limit).

Terminal void ratios for constant peak amplitude cyclic shear are strain level and confining pressure dependent. The fastest rate of densification would be achieved by straining the soil to the strain at the characteristic state in each cycle.

The most pronounced volumetric strains occur during early stages of the process, and gradually diminish as the medium asymptotically approaches its terminal density. An exponential function properly fits the evolution in void ratio with the number of events, from the initial void ratio to the terminal void ratio. The exponent α indicates the rate of convergence towards the terminal void ratio e_T . The inverse, $1/\alpha$, is the number of cycles required to reduce the difference between the current void ratio e_0 and the terminal void ratio by ~63%.

Values of $1/\alpha$ appear to be much greater than 1 in liquefaction–densification processes. Therefore a large number of liquefaction events can take place at the same site: that is, additional liquefaction events should be expected at a given site that has already liquefied.

The terminal density framework accommodates known processes (e.g. critical state in monotonic shear) and procedurally defined bounds (e.g. e_{\min} and e_{\max}), and it can be used for the optimal design of processes such as vibratory compaction and blast densification.

ACKNOWLEDGEMENTS

Support for this research was provided by the National Science Foundation, the Mid-America Earthquake Center and the Goizueta Foundation.

NOTATION

- CSL critical-state line
- C_u uniformity coefficient
- D_{50} mean particle size diameter
- e void ratio
- e_0 initial void ratio
- e_{cs} critical-state void ratio
- e_i void ratio at the i th event

- e_{\max} maximum void ratio
- e_{\min} minimum void ratio
- e_T terminal void ratio
- $e^{1 \text{ kPa}}$ critical-state void ratio at 1 kPa
- $e_{cs,0}^>$ specimen initial void ratio before the first cyclic event
- G_s specific gravity
- H height
- ID inner diameter
- I_r rigidity index in the NorSand model
- i event count
- $i_{63\%}$ event count to achieved 63% of terminal condition
- p' mean effective stress
- p'_0 initial mean effective stress
- q deviatoric stress
- u_e excess pore water pressure
- α convergence rate towards terminal void ratio
- γ_w unit weight of water
- ϵ_a axial strain
- λ critical-state line slope (given in logarithm base 10)
- ν Poisson’s ratio
- ϕ_{cs} critical-state friction angle

REFERENCES

Bement, R. A. P. & Selby, A. R. (1997). Compaction of granular soils by uniform vibration equivalent to vibrodriving of piles. *Geotech. Geol. Engng* **15**, No. 2, 121–143.

Buchanan, M. (2003). Think outside the sandbox. *Nature* **425**, No. 6958, 556–557.

Casagrande, A. (1936). Characteristics of cohesionless soil affecting the stability of slopes and earth fills. *J. Boston Soc. Civ. Engng*, 13–32.

Castro, G. (1969). *Liquefaction of sands*, Harvard Soil Mechanics Series No. 81. Cambridge, MA: Harvard University.

Chantawarangul, K. (1993). *Numerical simulations of three-dimensional granular assemblies*. PhD dissertation, University of Waterloo.

Corwin, E. I., Jaeger, H. M. & Nagel, S. R. (2005). Structural signature of jamming in granular media. *Nature* **435**, No. 7045, 1075–1078.

Cudmani, R. & Gudehus, G. (1999). Settlements of sand due to cyclic twisting of a tube. *Proceedings of the IUTAM symposium on theoretical and numerical methods in continuum mechanics of porous materials* (ed. W. Ehlers), pp. 387–396. Stuttgart: Kluwer Academic.

Dafalias, Y. F. (1993). Overview of constitutive models used in VELACS. *Proceedings of the international conference on the verification of numerical procedures for the analysis of soil liquefaction problems*, Davis, CA, Vol. 2, pp. 1293–1304.

Desrues, J., Chambon, R., Mokni, M. & Mazerolle, F. (1996). Void ratio evolution inside shear bands in triaxial sand specimens studied by computed tomography. *Géotechnique* **46**, No. 3, 529–546.

Drabkin, S., Lacy, H. & Kim, D. S. (1996). Estimating settlement of sand caused by construction vibration. *J. Geotech. Engng ASCE* **122**, No. 11, 920–928.

Fiegel, G. L. & Kutter, B. L. (1994). Liquefaction mechanism for layered soils. *J. Geotech. Geoenviron. Engng ASCE* **120**, No. 4, 737–755.

Herrera, M. C., Lizcano, A. & Santamarina, C. (2006). Colombian volcanic ash soils. In *Proc. 11th Int. Workshop on Characterization and Engineering Properties of Natural Soils* (eds T. S. Tan, K. K. Phoon, D. W. Hight and S. Leroueil), pp. 2385–2409. Taylor & Francis.

Ishihara, K. (1985). Stability of natural deposits during earthquakes. *Proc. 11th Int. Conf. Soil Mech. Found. Engng, San Francisco* **2**, 321–376.

Ishihara, K. (1996). *Soil behaviour in earthquake geotechnics*. Oxford: Oxford University Press.

Ishihara, K., Tatsuoka, F. & Yasuda, S. (1975). Undrained deformation and liquefaction of sand under cyclic stresses. *Soils Found.* **15**, No. 1, 29–44.

Jefferies, M. G. & Shuttle, D. A. (2002). Dilatancy in general Cambridge-type models. *Géotechnique* **52**, No. 9, 625–638.

Jefferies, M. G. & Shuttle, D. A. (2005). NorSand: features,

- calibration and use. In *Soil constitutive models: evaluation, selection, and calibration*, Geotechnical Special Publication 128 (eds J. A. Yamamuro and V. N. Kaliakin), pp. 204–236. Reston, VA: ASCE.
- Kokusho, T. & Kojima, T. (2002). Mechanism for post liquefaction water film generation in layered sand. *J. Geotech. Geoenviron. Engng ASCE* **128**, No. 2, 129–137.
- Lackenby, J., Indraratna, B., McDowell, G. & Christie, D. (2007). Effect of confining pressure on ballast degradation and deformation under cyclic triaxial loading. *Géotechnique* **57**, No. 6, 527–536.
- Lee, J. S. & Santamarina, J. C. (2007). Seismic monitoring short-duration events: liquefaction in 1g models. *Can. Geotech. J.* **44**, No. 6, 659–672.
- Luong, M. P. (1980). Stress–strain aspects of cohesionless soils under cyclic and transient loading. *Proceedings of the international symposium on soils under cyclic and transient loading*, Swansea, pp. 315–324.
- Mueth, D. M., Debregeas, G. F., Karczmar, G. S., Eng, P. J., Nagel, S. R. & Jaeger, H. M. (2000). Signatures of granular microstructure in dense shear flows. *Nature* **406**, No. 6794, 385.
- Narin van Court, W. A. & Mitchell, J. K. (1998). *Investigation of predictive methodologies for explosive compaction*, Geotechnical Special Publication No. 75, pp 639–653. Reston, VA: ASCE.
- Nowak, E. R., Knight, J. B., Ben-Naim, E., Jaeger, H. M. & Nagel, S. R. (1998). Density fluctuations in vibrated granular materials. *Phys. Rev. E* **57**, No. 2, 1971–1982.
- Oda, M. & Kazama, H. (1998). Microstructure of shear bands and its relation to the mechanics of dilatancy and failure of dense granular soils. *Géotechnique* **58**, No. 4, 465–481.
- Özkan, M. Y., Tunçer, M. A. & Yılmaz, Ç. (1996). An evaluation of Sürgü dam response during 5 May 1986 earthquake. *Soil Dynam. Earthquake Engng* **15**, 1–10.
- Santamarina, J. C. (2002). Soil behavior at the microscale: particle forces, soil behavior and soft ground construction. In *The Ladd Symposium*, ASCE Special Publication 119 (eds J. T. Germaine, T. C. Sheahan and R. V. Whitman), pp. 25–56. Reston, VA: ASCE.
- Santamarina, J. C., Klein, K. A. & Fam, M. A. (2001). *Soils and waves: particulate materials behavior, characterization and process monitoring*. Chichester/New York: J. Wiley & Sons.
- Savage, S. B. (1994). The mechanics of rapid granular flows. *Adv. Appl. Mech.* **24**, 289–365.
- Schofield, A. N. & Wroth, P. (1968). *Critical state soil mechanics*. London: McGraw-Hill.
- Scott, R. F. (1986). Solidification and consolidation of a liquefied sand column. *Soils Found.* **26**, No. 4, 23–31.
- Seed, H. B. & Silver, M. L. (1972). Settlement of dry sands during earthquakes. *J. Soil Mech. & Found. Div. ASCE* **98**, No. 4, 381–397.
- Soga, K. (1998). Soil liquefaction effects observed in the Kobe earthquake of 1995. *Proc. Instn Civ. Engrs Geotech. Engng* **131**, No. 1, 34–51.
- Taylor, D. W. (1948). *Fundamentals of soil mechanics*. New York: Wiley.
- Tokimatsu, K. & Seed, H. B. (1987). Evaluation of settlements in sands due to earthquake shaking. *J. Geotech. Engng ASCE* **113**, No. 8, 861–878.
- Umbanhowar, P. (2003). Granular materials: shaken sand—a granular fluid? *Nature* **424**, No. 6951, 886–887.
- van Hecke, M. (2005). Granular matter: a tale of tails. *Nature* **435**, No. 23, 1041–1042.
- Vucetic, M., Dobry, R. J. O. G. & Eng, A. (1991). Effect of soil plasticity on cyclic response. *J. Geotech. Engng ASCE* **117**, No. 1, 89–107.
- Youd, T. L. (1984). Recurrence of liquefaction at the same site. *Proc. 8th World Conf. on Earthquake Engineering, San Francisco* **3**, 231–238.